JASA ARTICLE

# Numerical modeling of Mach-stem formation in high-amplitude time-reversal focusing

Brian D. Patchett,[a] Brian E. Anderson, and Adam D. Kingsley
*Acoustics Research Group, Department of Physics and Astronomy, Brigham Young University, Provo, Utah 84602, USA*

**ABSTRACT:**
In acoustics, time-reversal processing is commonly used to exploit multiple scatterings in reverberant environments to focus sound to a specific location. Recently, the nonlinear characteristics of time-reversal focusing at amplitudes as high as 200 dB have been reported [Patchett and Anderson, J. Acoust. Soc. Am. **151**(6), 3603–3614 (2022)]. These studies were experimental in nature and suggested that converging waves nonlinearly interact in the focusing of waves, leading to nonlinear amplification. This study investigates the nonlinear interactions and subsequent characteristics from a model-based approach. Utilizing both finite difference and finite-element models, it is shown that nonlinear interactions between high-amplitude waves lead to free-space Mach-wave coalescence of the converging waves. The number of waves used in both models represents a small piece of the full aperture of converging waves experimentally. Limiting the number of waves limits the number of Mach-stem formations and reduces the nonlinear growth of the focus amplitudes when compared to experiment. However, limiting the number of waves allows the identification of individual Mach waves. Mach wave coalescence leading to Mach-stem formation appears to be the mechanism behind nonlinear amplification of peak focus amplitudes observed in high-amplitude time-reversal focusing.  https://doi.org/10.1121/10.0017974

(Received 10 January 2023; revised 17 March 2023; accepted 7 April 2023; published online 3 May 2023)

[Editor: Yun Jing] Pages: 2724–2732

## I. INTRODUCTION

Time-reversal (TR) signal processing is a technique utilized in multiple fields of wave-based physics to focus sound to a chosen position in a given environment.[1–3] The TR process is composed of two primary steps to achieve this focusing. In the forward step, an impulse response (IR) is obtained from a source in the environment to a receiver. A swept sine wave, or "chirp" signal, may be used as the input signal. The receiver's response to this chirp signal is referred to as the chirp response (CR). The CR is the convolution of the environment IR with the input chirp. To extract the IR, the input chirp signal is cross-correlated with the CR to calculate the band limited IR of the environment. In this way, cross correlation can be viewed as a practical method of deconvolution to obtain an IR.[4,5]

In the second part of the TR process, called the backward step, the IR is reversed on the time axis (hence the name time reversal), creating the time-reversed impulse response (TRIR). The TRIR can be broadcast from the original source position, resulting in a convergence of sound waves onto the receiver and a focus of energy. Because the TR process utilizes reflections within the IR as virtual sources during the backward step, the TR process greatly benefits from reverberant environments when techniques such as beam forming do not benefit from the same environments. The time-symmetric focal signal[6] recorded at the receiver is equivalent to an auto-correlation of the IR.[7] The focused waves are, thus, impulsive in nature.

TR has been used in many applications. It began as a method of reproducible underwater communication that would be difficult to intercept during transmission.[8,9] TR focusing was applied as an effective means of kidney stone destruction via lithotripsy by utilizing an array of transducers known as a time-reversal mirror.[10] TR has also been used for the histotripsy destruction of tumors, biological soft tissues, and other inhomogeneous bio-materials.[11,12] It has been explored as a communication tool for audible sound in highly reverberant, airborne environments.[13,14] TR has also been studied as an effective method of focusing sound in different room environments.[15,16] The field of nondestructive evaluation of materials has used TR as an effective method of evaluation of defects, or cracks, in the material that can be identified by focusing to different locations in the material and observing differences in the nonlinear response of the focused waves.[3]

TR focusing of waves at high amplitudes has many promising applications. In a study conducted by Montaldo *et al.*,[17] the focusing of sound waves in an underwater environment was characterized. They showed that as TRIR amplitudes were increased, the characteristics of the focus waveform noticeably changed. Nonlinear attributes, including shock wave formation, harmonic generation, and reduction of peak amplitudes relative to linear scaling, were observable in their work. A study done by Willardson *et al.*[18] made preliminary observations of a small nonlinear increase in the peak amplitude of the focus generated using TR of airborne,

[a]Electronic mail: brian.patchett@uvu.edu

https://doi.org/10.1121/10.0017974

audible sound at very loud sound levels (this is discussed more below). High-amplitude focusing of ultrasound was studied by Wallace and Anderson,[19] who showed that when ultrasonic waves in two primary frequency bands are co-focused at high levels, a difference frequency in the audible acoustic range can be generated. Recently, Patchett and Anderson[20] characterized the nonlinear features present in the signal when focusing at levels as high as 200 dB. They observed significant nonlinear amplification of peak amplitudes in the TR focusing and described a potential mechanism by which the nonlinearities were generated, known as free-space Mach-stem formation. Waveform steepening was also observed, although this did not seem to be the cause of the nonlinear amplification of compression peaks. These effects were studied and characterized primarily through experimental methods.

In addition to these studies of nonlinearities in TR focusing, several studies have aimed at maximizing the peak focus amplitude in TR. Derode *et al.*[21] introduced one-bit signal processing (a form of intentional clipping of the TRIR) to obtain a 12 dB increase in amplitude in an underwater experiment, albeit at the expense of focus quality. In a study done by Heaton *et al.*,[22] a variant of one-bit processing known as clipping, which preserves more energy in the TRIR, leading to higher amplitude focusing, was investigated in solid materials. They were able to show an increase in peak focus amplitude employing the clipping method when compared to other TR methods, including one-bit processing. Anderson *et al.*[5] showed that the peak focus amplitude could also be increased by pointing the sources away from the receiver position in a reverberant environment, which increased the peak amplitude of the focus signal. Denison and Anderson[23] found that smaller volume rooms result in larger focusing amplitudes, although previous studies had predicted that shorter reverberation times (smaller rooms have shorter reverberation times) should decrease the amplitude. This finding was partly confirmed by Patchett *et al.*,[24] who also showed that when the TR focusing occurs near walls, edges, and corners of a room, the focal amplitude increases. In a separate study, Denison and Anderson[25] found that placing sources further away from the focal location (at distances greater than the room's critical distance), placing sources in the same plane as the focusing, and increasing the angular aperture (rather than using sources in a line array) all contributed to a larger focal amplitude. A comparison of TR signal processing methods was done by Willardson *et al.*,[18] demonstrating that the clipping method was the most effective TRIR preprocessing technique to employ for maximizing the peak focus amplitude when focusing audible sound in air. Young *et al.*[26] conducted a similar investigation for applications using ultrasound within solid materials, arriving at the same conclusion.

This paper presents further work on high-amplitude (often called finite amplitude) focusing of sound through the creation of two types of models to compare qualitatively with the results seen experimentally by Patchett and Anderson.[20] The first model was designed using a well-known MATLAB® (Natick, MA) package called k-Wave®.[27,28] The second type of model employed finite-element modeling using the COMSOL Multiphysics® (Burlington, MA) software package. These models demonstrate that, in addition to qualitatively verifying the characteristic nonlinearities already observed experimentally, free-space Mach-stem formation is the primary contributor to the nonlinear amplitude growth observed by Willardson *et al.*[18] and by Patchett and Anderson.[20]

Both models show that when nonlinearity is accounted for in the propagation of the waves, the wavefronts do indeed coalesce to form a region of higher overall pressure than expected with linear superposition and corresponding higher wave speeds of these finite amplitude waves. The k-Wave® model results indicate that a nonlinear increase relative to linearly scaled amplitudes in focused acoustic waves is present only when multiple high-amplitude acoustic waveforms are emitted. The waveforms also arrive earlier in time and become steeper on their leading edges as the TRIRs are amplified, due to waveform steepening. The waveform steepening also nonlinearly increases the high frequency content of the waves. The results of the COMSOL® modeling clearly show the formation of individual free-space Mach-stem events where the waves have coalesced to form higher than expected (relative to linear superposition) pressure wave fronts. These Mach stems travel at faster wave speeds than the direct waves, and eventually the Mach stems and the direct waves coalesce to form one large wave front with peak amplitudes that are nonlinearly larger in amplitude than linearly scaling would predict. The peak focus amplitudes reported by the models are not as high as amplitudes measured in experiments, but the difference is caused by limiting the number of waves coalescing in the TR focusing. This limit occurs because virtual sources were not utilized in these free-space models in order to simplify the models, reduce computation time, and observe the formation of individual Mach stems. In other words, the models only include the direct sound emissions of the TR process since inclusion of all of the reflections, modeled as image sources, would require an impossibly large modeling domain. By modeling far fewer converging waves, the same trends are still observed, and the formation of the individual, free-space Mach stems can actually be observed to clearly identify the nonlinear mechanism responsible for the nonlinear peak growth observed in experiments.

## II. k-WAVE® MODEL DESIGN

k-Wave® is an open-source package that accounts for nonlinear wave propagation in custom scenarios. It employs a combination of the finite difference method (for times steps) and the k-space pseudospectral method (for spatial gradients). The k-space pseudospectral method is a frequency domain approach to solving the fundamental first-order differential equations that are typically combined

to generate the wave equation, which is a second-order partial differential equation. When combined in their nonlinear form, the equations can be used to create a generalized form of the Westervelt equation.[29] Jing *et al.*[30] was able to verify that a generalized form of the Westervelt equation was a valid method for simulation of focused sources. The pseudospectral method that k-Wave® employs has been shown to provide faster computational processing through implementation of a correction operator. Treeby *et al.*[31] showed that the correction operator within the pseudospectral method accurately models the superposition of waves at any angle of incidence, which is important for our model. The accuracy is limited by the bandwidth of the signal; a band limited signal will contain less computational dispersion.[32] The model considered here employs the default k-Wave® pulse. This band limited pulse extends from 1 to 1500 Hz, peaking at 450 Hz.

The k-Wave® package allows the user to place a series of sources and receivers in any three-dimensional configuration desired in a free-space environment. The properties of the environment are input independently to allow the user to define parameters such as density, sound speed, and the B/A nonlinear parameter used in nonlinear acoutics.[33] Using these parameters, models can be generated in any type of fluid, and the degree of nonlinearity may be modified. A perfectly matched layer (PML) boundary condition is defined to allow for the waves to propagate out of the defined area without reflection or undesirable interactions at the boundaries. At high amplitudes, waves traveling parallel along the boundaries did prove to create very small unnatural fluctuations near the PML, although this effect was minimal. Nonlinear wave propagation is controlled by entering the appropriate B/A value for the fluid. This nonlinear term can also be removed from the calculation for a direct comparison to linearly propagating waves. Utilizing these functions, it is then possible to simulate the convergence of high-amplitude waves as they propagate to a focus position from an array of receivers that are equally spaced from the focus location.

To explore the interaction between high-amplitude waves, a simple model was constructed in the k-Wave® open-source software. A circular array of 18 sources was placed on a plane, along with a linear array of 121 receivers. The receiver was oriented at the center of the $x$ and $y$ axes, and the sources were placed in such a way that they formed a full 360° circle about the array, with the center receiver being located at the center of the circle of sources (see Fig. 1). A radial distance of 5 m from each source to the central receiver was used and a source radius of 0.25 m. k-Wave® requires a finite-sized user-defined source radius, which we chose through trial and error to create a strong source wave without disrupting the PML boundary. To generate the desired large amplitude waves, if the source is too small, then its velocity must exceed the speed of sound, which is why the sources have their finite extent. This geometry allows for focusing of the array to the central receiver (from here on referred to as the focus location).

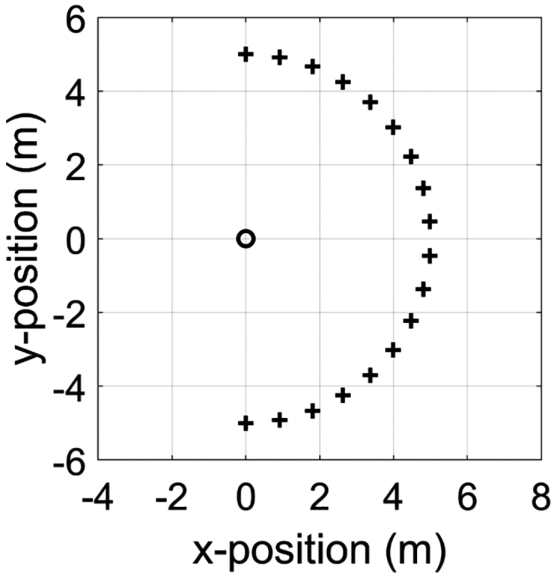


FIG. 1. Layout of sources (+) and receivers (○) in the initial 360° k-Wave® model.

### A. Nonlinear features of TR focusing as a function of array aperture

A single pulse is sent from each source simultaneously with equal initial pressure amplitude. The pulses all arrive at the focus location simultaneously, creating a focus wave similar in characteristics to a focus generated using TR in free space. To determine whether the angle of incidence would affect the peak pressure measured at the focus location, the 18 sources are then moved to fit within a 180° aperture. The model is repeated, and the results are compared to determine whether a closer angle of incidence would increase the amplitudes of the focal signals more than when a 360° aperture is used. Placement of the sources is limited to intersections of the grid spacing defined in the model. As such, the number of angles that would provide an equal distance from each source to the receiver is limited as well. The angles used were chosen because the grid spacing allowed for the best placement of the sources. The initial source pressure amplitude broadcast from each source was 12 000 Pa, and the nonlinear parameter of B/A was set to 0.4 for air. Figure 2 shows that as the angular spacing between sources is decreased, steepening of the converging wave begins to increase. The peak amplitude occurs at the total aperture angle of 106° ± 17°. The error value is due to the limited placement options of the sources, which limits the angles that can be tested. The ± error value represents half of the difference between 140° and 106° and half of the difference between 106° and 73°.

The total aperture angle was decreased in eight increments, 180°, 155°, 140°, 106°, 73°, 56°, 46°, and stopping at a total aperture angle of 32° as this was the limit in which the sources would fit without overlapping each other in the model. The peaks for the lowest three angles continued to decrease in amplitude and are omitted from Fig. 2 to allow for clarity in the figure. To determine the amount of peak

https://doi.org/10.1121/10.0017974

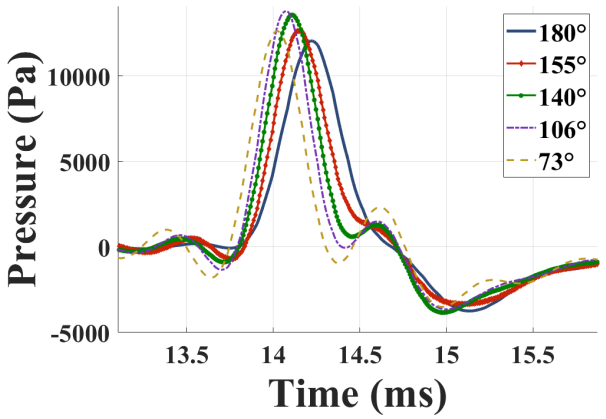


FIG. 2. (Color online) Comparison of five example focus signals at the focus location as the total aperture angle of the 18 sources is changed.

pressure increase caused by the change in aperture angle of the 18 sources, the model was run again with the nonlinear parameter (B/A) removed from the k-Wave® function inputs. Then a comparison of the nonlinear peak amplitudes to the linear peak amplitudes at each aperture angle can be calculated. As expected, the linear model yielded focus signal amplitudes and waveforms that were identical to every other linear broadcast, irrespective of angle, because each source only contributes the primary direct sound wave amplitudes to the focus. The results of a ratio comparison of the nonlinear to linear results are shown in Fig. 3.

The greatest increase in peak pressure due to nonlinearity happens at a total aperture angle of 106° ± 17°, or an optimal source separation angle of ∼6° between adjacent sources. Vaughn *et al.*[34] explored the Mach stems formed by ground reflections of jet noise and their dependence on the so-called critical parameter (that stems from the Khokhlov–Zabolotskaya equation).[35] Using half of the angular separation of the sources in Eq. (1) from Vaughn *et al.* to calculate the variable $a$, which is defined as the approximate critical parameter, for the wave amplitudes considered here yields values of around $a \approx 0.2$. This suggests that these wave amplitudes fall within the weak von Neumann regime, which implies that the ability to see Mach reflections of the waves is possible.

Two metrics for quantifying the degree of wave steepening of the focused waves were employed to show that the change in aperture angle also affects the steepening of the wavefronts generated at the focus location. First, the time of arrival of the peak pressure at the focus location is compared to the total aperture angle for the sources, shown in Fig. 4.

From these data, we can see that as the total aperture shifts from 360° to 73°, the wavefront advances forward in time, arriving earlier at the focus location. As the total aperture decreases below 73°, the effect of wave steepening decreases. Thus, a total aperture of 73° (+17°/–8.5°) (an angular spacing of 4° between adjacent sources) yields the largest wave steepening effects.

The second metric used to monitor the differences in wave steepening is the maximum value of the temporal derivative of each time waveform on the leading edge of the wave. These maximal slope values are plotted versus total aperture angle in Fig. 5. Again, a total aperture angle of 73° (+17°/–8.5°) yields the largest slope due to waveform steepening. The largest slope occurring at a total aperture angle of 73° (+17°/–8.5°) could be an indication that when the adjacent sources are closer than ∼4° to each other, there is no longer the opportunity for free-space Mach stems to form because the sources are so close together that their emitted waves are propagating along coincident paths. These angles are only approximate (due to the finite grid spacing) and can only be assumed for the two-dimensional case described by the model. A more empirical value for them in a real reverberant environment remains to be found.

Using the total angular aperture that generated the maximum nonlinear waveform steepening increase, we now show the increase in peak amplitude and waveform steepening as a function of the amplitude of the source pulses, just as was done in the experiment outlined in Patchett and Anderson.[20] The total aperture for the 18 sources was set to a constant 73°, and the pressure is increased from 2 to 12 kPa in increments of 2 kPa. These values were chosen because the linear superposition of 18 waves with an initial

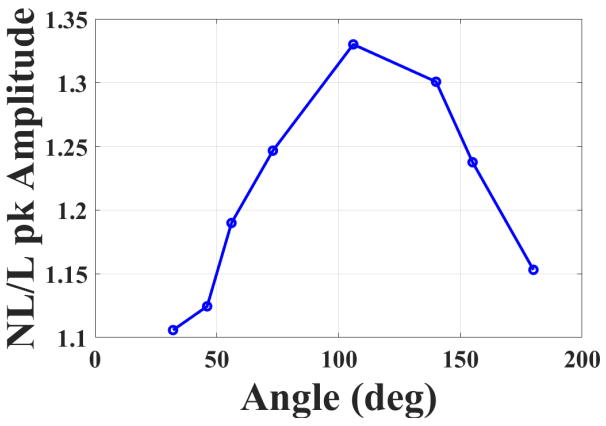


FIG. 3. (Color online) Ratio of the peak amplitudes for the nonlinear (NL) and linear (L) models as a function of total aperture angle.

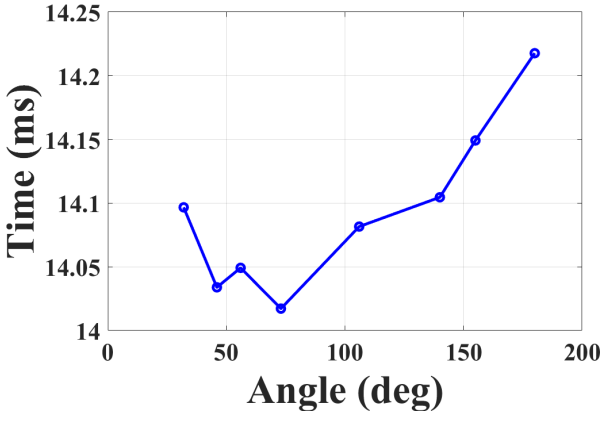


FIG. 4. (Color online) Comparison of the time at which the peak pressure point arrives at the focus location versus the total aperture angle that the 18 sources are arranged in.

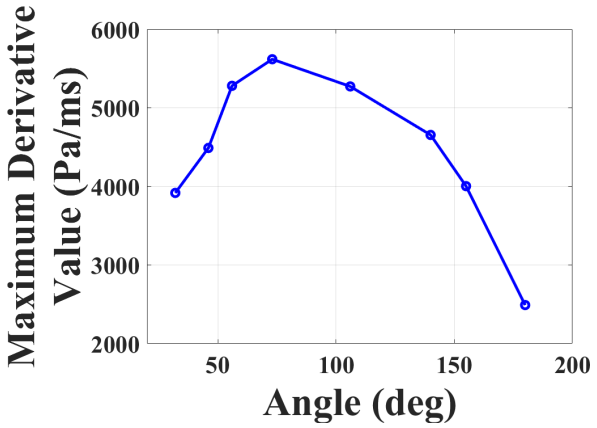


FIG. 5. (Color online) Comparison of the temporal derivative of the leading edge of the focusing wave at the focus location versus the total aperture angle that the 18 sources are arranged in.

source pressure value of 2000 Pa would linearly superpose at the focus to a sound pressure level of 174 dB. The experimental studies done by Willardson *et al.*[18] and Patchett and Anderson[20] indicate this level can be considered the threshold where nonlinear amplification of peak pressures begins for converging waves created using TR. Figure 6 shows the focal signals recorded at the focus.

Each data set is scaled linearly by a constant value to show the relative nonlinear changes, such as the nonlinear increase in the peak amplitude as the source pressure is increased. As shown experimentally, increasing the output level of the sources does lead to an increasing level of nonlinear interactions between the waves as they converge at the focal location. Although not reported here, the spectrum of the focal signals also shows a nonlinear increase in high frequency content, as was also observed experimentally, which is a sign of waveform steepening.

### B. Focusing with acoustic superposition versus post-processing superposition

In addition to the models outlined above, a recreation of the methods of focus generation outlined in Sec. III D of Patchett and Anderson[20] was simulated for comparison using k-Wave®. In this model, eight sources are arranged into a circular array with the same geometric dimensions used in Sec. II A, with each source placed 45° from its neighbor. The initial source pressure of each is set to 25 kPa. For the first part of the experiment, the eight source broadcasts are done simultaneously, thereby summing together acoustically. In the second part, the eight source broadcasts are done individually, and the results are summed electronically in post-processing. The experiment now recreates the aforementioned experiment from Patchett and Anderson[20] that ensures that the nonlinear effects are in fact a direct result of the acoustic mixing of the focus signals. Figure 7 shows the two resulting focus signals.

Figure 7 clearly shows that when the signals are generated simultaneously, the nonlinear acoustic effects are more pronounced, with the focus having a higher amplitude, arriving sooner in time, and having a steeper leading edge than it would if the signals were linearly superposed with each other. The result agrees with the experimental data from Patchett and Anderson,[20] although the effect appears to a greater extent in the experimental results due to the higher number of virtual sources from reflections in the reverberation chamber. Calculating the change in the nonlinear amplitude-dependent wave speed in the model for the acoustically mixed signal shows that a peak temperature increase of 2 °C occurs as the peak of the wave propagates. This temperature increase would allow the wave to propagate at such a speed that it would arrive 3 ms sooner than the linearly summed waves, which is the time difference seen in Fig. 7.

## III. COMSOL MULTIPHYSICS® MODEL DESIGN

In addition to the k-Wave® model, a similarly simple model was designed in COMSOL Multiphysics® to visualize individual Mach-stem formations in the focused waves for comparison to the k-Wave® results in two and three dimensions. Linear and nonlinear propagation simulations

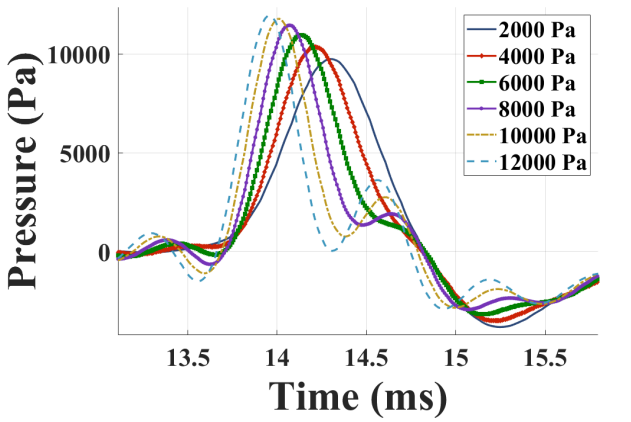


FIG. 6. (Color online) Linearly scaled focus peaks at a fixed total aperture angle of 73°, as the output pressure of the source is increased.

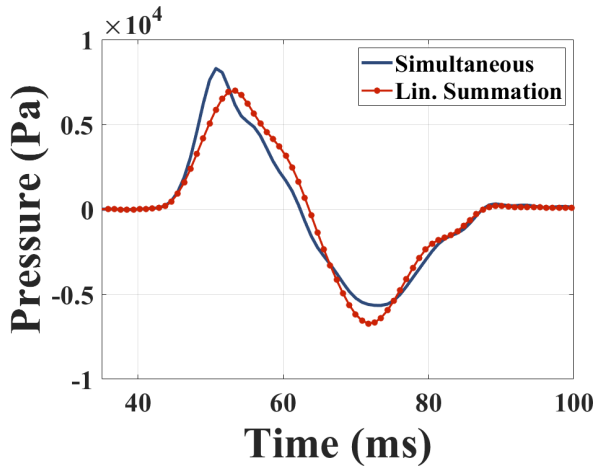


FIG. 7. (Color online) A comparison of the linearly summed signals (summed in post-processing) from each source in the k-Wave® model, to the field created when all of the sources generate their signals simultaneously.

https://doi.org/10.1121/10.0017974

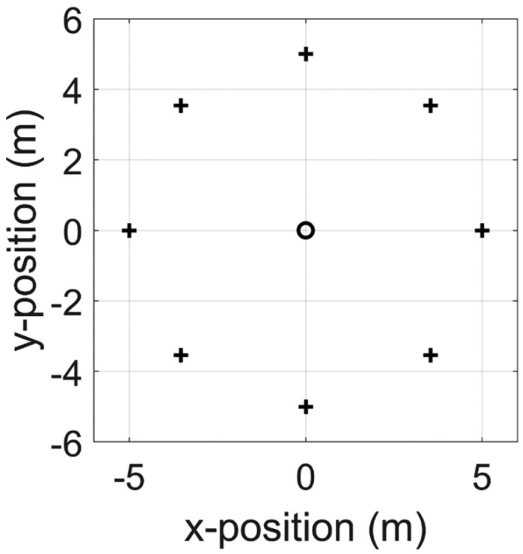


FIG. 8. Arrangement of sources (+) and receiver (○) for the COMSOL Multiphysics® model of high-amplitude wave interference.

were conducted. The design of the model matched the dimensions and geometry of the k-Wave® model. The pulse source signal used was made to be the same as that used with the k-Wave model. Specifically, the radial distance from each source to the center point where the waves converge is 5 m, and each source has a radius of 0.25 m. To better visualize the interaction of the overlapping high-amplitude pulses, eight sources were placed equidistant from a central receiver (also referred to as the focus location here), in a circular arrangement with each source placed 45° from the adjacent sources. Figure 8 shows the geometry of the arrangement. This arrangement benefits from COMSOL's ability to capture an entire field with a high-resolution mesh grid. With the sources at a larger angle of incidence from each other, it is possible to view the individual interactions of overlapping waves with greater detail as they propagate across the region toward the focus location. The software allows observations of individual Mach wave coalescence events and shows that they contribute to the nonlinear amplification of the peak focus amplitude by arriving at the same time as the initial wave.

The COMSOL® package applies the lossy Westervelt equation, which includes a term for diffusive loss due to propagation and employs fewer assumptions about the nonlinear propagation of waves than does the pseudospectral method. However, it is assumed that both equations are valid for our modeling. The Westervelt equation is known to accurately represent the cumulative effects of the intersecting waves far from the sources. This ability makes COMSOL® a good choice for calculating the complex interactions of the waves as they propagate.[30] The Westervelt equation is known to struggle in modeling the near field of sources. Fortunately, our results are not dependent on accuracy in the near field of the sources. COMSOL® utilizes a highly complex finite-element mesh grid to create the desired geometry of a space and the desired boundary conditions. Thus, it is more computationally efficient at simultaneously modeling the entire propagating wave field than k-Wave, which is intended to calculate the field at user-defined, discrete positions. The COMSOL® software then displays a time waveform animation of the propagating waves. These abilities make COMSOL® an excellent platform for viewing the spatial extent of wave interactions in high resolution.

The images in Figs. 9 and 10 are shown at the same time intervals after source emissions, for linear and nonlinear models, respectively, to demonstrate that including nonlinear propagation significantly increases the speed of the converging waves. Figures 9(a)–9(c) and 10(a)–10(c) show the source locations as the array of white circles placed equidistant from the center of the array. The initial waves propagating outward are shown in dark gray [Fig. 9(a)], with the overlapping regions shown in light gray (constructive interference). Figure 9(b) shows an image 0.7 ms later in time. Additional regions of overlap have happened as the

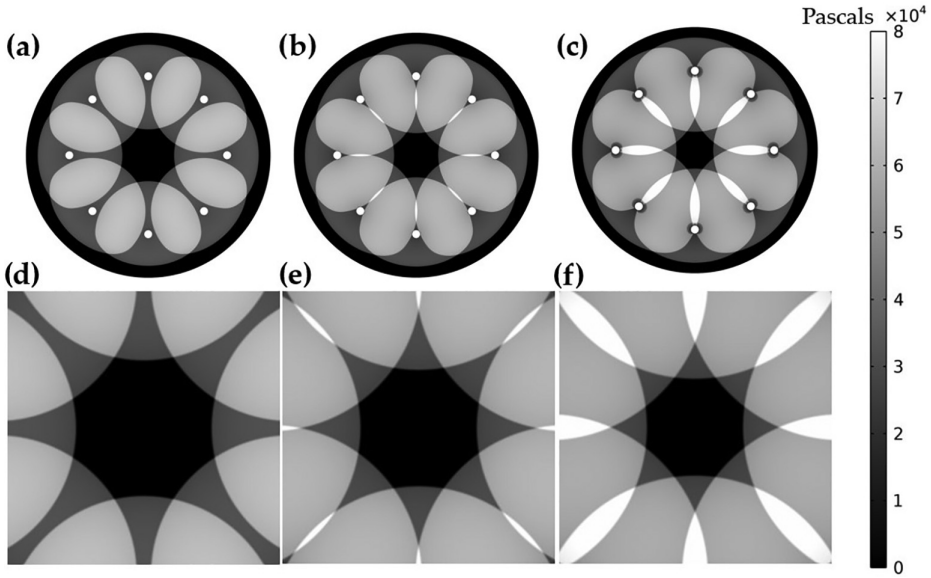


FIG. 9. COMSOL® images of linear waves propagating from the eight sources. The top row [(a)–(c)] shows the full view of the modeled region at 9.3, 10.0, and 10.3 ms, respectively, whereas the second row [(d)–(f)] shows blown-up images of the center of each above image, respectively.

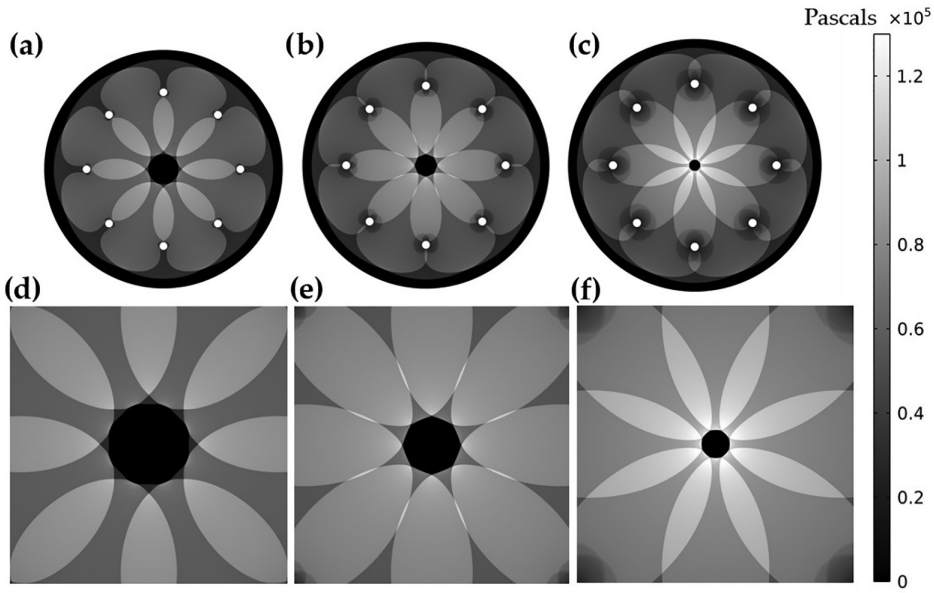


FIG. 10. COMSOL® images of nonlinear waves propagating from the eight sources. The top row [(a)–(c)] shows the full view of the modeled region at 9.3, 10.0, and 10.3 ms, respectively, whereas the second row [(d)–(f)] shows blown-up images of the center of each above image, respectively.

waves converge to the center. Finally, the last image [Fig. 9(c)] shows the propagation an additional 0.7 ms later in time and has multiple regions of overlap as the waves propagate into the center. The primary purpose of the zoomed in images [Figs. 9(d)–9(f)] is to show that the leading edge of the converging waves continues to have a convex shape that maintains a very distinct point where the waves overlap. Essentially, Fig. 9 shows that the pressures arriving at the focus are simply the linear superposition of the individual broadcasts; the shape of the leading edge of the wave is not changed, nor is the expected peak pressure nonlinearly amplified when it reaches the focus.

A comparison of Figs. 9 and 10 shows that the waves in the nonlinear model are traveling faster than the waves in the linear model as evidenced by the smaller black void in the middle of the converging waves for the nonlinear model results. When looking at the zoomed in images of Figs. 10(d)–10(f), one can see that as the waves begin to converge, the overlapping regions of the leading edges generate a gradient of higher pressure where they interact with the adjacent waves (seen as light gray to white gradations in the overlap regions going left to right through the images). Figure 10 shows that free-space Mach waves are formed in this region; that, due to the finite amplitude of the coalescing waves, the wave speed of the overlapping amplitudes increases relative to the wave speed of the direct waves from the sources; and that these Mach waves eventually overtake the leading waves and dominate the resulting leading edge of the converging wave front.

Because Mach stems take over the leading wavefront, the pressure at the location of focusing has a higher peak amplitude than linear superposition would predict. As the wavefront converges, it also takes on a more circular shape due to the increased number of Mach coalesced wavefronts overtaking the initial leading wave. Figure 11 compares the circular shape formed in Fig. 10 with the convex wavefronts

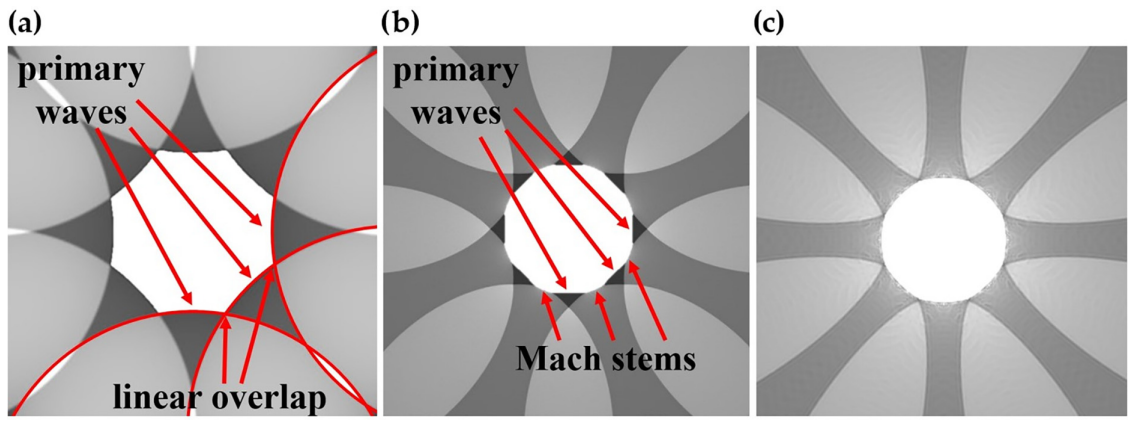


FIG. 11. (Color online) (a) A zoomed in view of Fig. 9(b) where the linear interaction of the wavefronts is clearly visible. (b) A zoomed in view of Fig. 10(a), which happens earlier in time than (a), where nonlinear propagation is accounted for and Mach stems begin to form between each adjacent pair of overlapping primary waves. (c) A zoomed in view of Fig. 10(c), where the nonlinear propagation has led to the Mach stem waves creating a circular convergence pattern. This image is later in time and not to scale with images (a) and (b). The color scale for these images is the same as the scales given for Figs. 9 and 10, respectively.

https://doi.org/10.1121/10.0017974

in Fig. 9. The black central color has been replaced with white to better show the wavefronts that are being compared. Specifically, Fig. 11(a) is a closer look at the linear waves in Fig. 9(b), with the addition of some markers to help the reader clearly identify the waves presented. The waves labeled "primary waves" in Fig. 11(a) are the initial waves that emanated from the sources.

The curvature of three of these waves is outlined to illustrate better the entire wavefront propagating from each source. The points labeled as "linear overlap" are the points of intersection between the primary waves, where they begin to overlap. In Fig. 11(b), we see a zoomed in look at the nonlinearly propagating waves shown in Fig. 10(a). The initial wavefronts are again labeled as "primary waves." The difference in this image is that where the points of intersection should be, a high-pressure Mach stem has begun to form. These are labeled as "Mach stems." This figure more clearly illustrates the differences between the linear superposition of the waves and the nonlinear superposition of them when all other variables are held the same. In Fig. 11(c) we see a closer view of Fig. 10(c), where the nonlinear high-amplitude waves have converged to form a circle almost completely composed of Mach stems. This circle we have termed the "Mach ring," due to its ring-like appearance and the fact that the wavefront is now almost entirely composed of converging Mach stems.

## IV. CONCLUSION

The results from the k-Wave® model, while limited in scope, show direct evidence that the convergence of high-amplitude waves to a focus location leads to a similar nonlinear increase in peak amplitudes as seen in experimental data by Patchett and Anderson.[20] It is clear that when finite amplitude waves are focused, the peak focus amplitude increases nonlinearly and shifts forward in time. This verifies qualitatively that the nonlinear increases seen in the experimental results are not the result of equipment artifacts. The k-Wave® model recreation of the experiment conducted by Patchett and Anderson[20] further verifies that a nonlinear acoustic mixing of the waves leads to the nonlinear increase in the peak focus amplitude as the waves converge. The results support the free-space Mach-stem hypothesis that the converging waves are interacting in such a way that peak focus amplitudes are nonlinearly larger than linear superposition would predict. This interaction was hypothesized by Patchett and Anderson.[20]

This free-space Mach-stem hypothesis was confirmed with modeling done in COMSOL Multiphysics®. The geometric arrangement and ability to finely mesh the region of focusing allowed for clear high-resolution images of the formation of Mach stems. These models showed that Mach-stem formations in free space do indeed occur when high-amplitude waves converge toward a focus location. The effect is so dramatic that the coalescing waves become the primary contributions to the circular wavefront that reaches the focal location, overtaking the initial wavefronts produced by the sources and creating the phenomenon termed a "Mach ring" of convergence. Wave steepening is observed in both of the two models, which results in the peak focal amplitude arriving earlier in time and with a steeper leading edge of the peak wave. These two modeling methods have also confirmed that the formation of free-space Mach stems through Mach wave coalescence also occurs and is the mechanism behind the nonlinear amplification of the focus peak growth seen in the high-amplitude TR focusing reported by Willardson *et al.*[18] and Patchett and Anderson.[20]


[1]M. Fink, "Time reversed acoustics," Phys. Today **50**(3), 34–40 (1997).
[2]B. E. Anderson, M. Griffa, C. Larmat, T. J. Ulrich, and P. A. Johnson, "Time reversal," Acoust. Today **4**(1), 5–16 (2008).
[3]B. E. Anderson, M. C. Remillieux, P.-Y. L. Bas, and T. J. Ulrich, "Time reversal techniques," in *Nonlinear Acoustic Techniques for Nondestructive Evaluation*, 1st ed., edited by T. Kundu (Springer, New York, 2018), pp. 547–581.
[4]B. Van Damme, K. Van Den Abeele, Y. Li, and O. Bou Matar, "Time reversed acoustics techniques for elastic imaging in reverberant and non-reverberant media: An experimental study of the chaotic cavity transducer concept," J. Appl. Phys. **109**(10), 104910 (2011).
[5]B. E. Anderson, M. Clemens, and M. L. Willardson, "The effect of transducer directivity on time reversal focusing," J. Acoust. Soc. Am. **142**(1), EL95–EL101 (2017).
[6]T. J. Ulrich, M. Griffa, and B. E. Anderson, "Symmetry-based imaging condition in time reversed acoustics," J. Appl. Phys. **104**(6), 064912 (2008).
[7]M. Tanter, J.-L. Thomas, and M. Fink, "Time reversal and the inverse filter," J. Acoust. Soc. Am. **108**(1), 223–234 (2000).
[8]A. Parvulescu and C. S. Clay, "Reproducibility of signal transmissions in the ocean," Radio Electron. Eng. UK **29**(4), 223–228 (1965).
[9]C. S. Clay and B. E. Anderson, "Matched signals: The beginnings of time reversal," Proc. Mtgs. Acoust. **12**(1), 055001 (2011).
[10]J.-L. Thomas, F. Wu, and M. Fink, "Time reversal focusing applied to lithotripsy," Ultrason. Imaging **18**(2), 106–121 (1996).
[11]M. Tanter, J.-L. Thomas, and M. Fink, "Focusing and steering through absorbing and aberrating layers: Application to ultrasonic propagation through the skull," J. Acoust. Soc. Am. **103**(5), 2403–2410 (1998).
[12]J.-L. Thomas and M. Fink, "Ultrasonic beam focusing through tissue inhomogeneities with a time reversal mirror: Application to transskull therapy," IEEE Trans. Ultrason. Ferroelect, Freq. Control **43**(6), 1122–1129 (1996).
[13]J. V. Candy, A. W. Meyer, A. J. Poggio, and B. L. Guidry, "Time-reversal processing for an acoustic communications experiment in a highly reverberant environment," J. Acoust. Soc. Am. **115**(4), 1621–1631 (2004).
[14]J. V. Candy, D. H. Chambers, C. L. Robbins, B. L. Guidry, A. J. Poggio, F. Dowla, and C. A. Hertzog, "Wideband multichannel time-reversal processing for acoustic communications in highly reverberant environments," J. Acoust. Soc. Am. **120**(2), 838–851 (2006).
[15]S. Yon, M. Tanter, and M. Fink, "Sound focusing in rooms: The time-reversal approach," J. Acoust. Soc. Am. **113**(3), 1533–1543 (2003).
[16]G. Ribay, J. de Rosny, and M. Fink, "Time reversal of noise sources in a reverberation room," J. Acoust. Soc. Am. **117**(5), 2866–28720 (2005).
[17]G. Montaldo, P. Roux, A. Derode, C. Negreira, and M. Fink, "Ultrasound shock wave generator with one-bit time reversal in a dispersive medium, application to lithotripsy," Appl. Phys. Lett. **80**, 897–899 (2002).
[18]M. L. Willardson, B. E. Anderson, S. M. Young, M. H. Denison, and B. D. Patchett, "Time reversal focusing of high amplitude sound in a reverberation chamber," J. Acoust. Soc. Am. **143**(2), 696–705 (2018).
[19]C. B. Wallace and B. E. Anderson, "High-amplitude time reversal focusing of airborne ultrasound to generate a focused nonlinear difference frequency," J. Acoust. Soc. Am. **150**(2), 1411–1423 (2021).
[20]B. D. Patchett and B. E. Anderson, "Nonlinear characteristics of high amplitude focusing using time reversal in a reverberation chamber," J. Acoust. Soc. Am. **151**(6), 3603–3614 (2022).

[21]A. Derode, A. Tourin, and M. Fink, "Limits of time-reversal focusing through multiple scattering: Long-range correlation," J. Acoust. Soc. Am. **107**(6), 2987–2998 (2000).
[22]C. Heaton, B. E. Anderson, and S. M. Young, "Time reversal focusing of elastic waves in plates for an educational demonstration," J. Acoust. Soc. Am. **141**(2), 1084–1092 (2017).
[23]M. H. Denison and B. E. Anderson, "Time reversal acoustics applied to rooms of various reverberation times," J. Acoust. Soc. Am. **144**(6), 3055–3066 (2018).
[24]B. D. Patchett, B. E. Anderson, and A. D. Kingsley, "The impact of room location on time reversal focusing amplitudes," J. Acoust. Soc. Am. **150**(2), 1424–1433 (2021).
[25]M. H. Denison and B. E. Anderson, "The effects of source placement on time reversal focusing in rooms," Appl. Acoust. **156**, 279–288 (2019).
[26]S. M. Young, B. E. Anderson, M. L. Willardson, P. E. Simpson, and P.-Y. Le Bas, "A comparison of impulse response modification techniques for time reversal with application to crack detection," J. Acoust. Soc. Am. **145**(5), 3195–3207 (2019).
[27]B. E. Treeby, J. Budisky, E. S. Wise, J. Jaros, and B. T. Cox, "Rapid calculation of acoustic fields from arbitrary continuous-wave sources," J. Acoust. Soc. Am. **143**(1), 529–537 (2018).
[28]B. E. Treeby, J. Jaros, D. Rohrbach, and B. T. Cox, "Modelling elastic wave propagation using the k-Wave MATLAB toolbox," in *Proceedings of the 2014 IEEE International Ultrasonics Symposium*, Chicago, IL (September 3–6, 2014), pp. 146–149.
[29]E. Martin, J. Jaros, and B. E. Treeby, "Experimental validation of k-Wave: Nonlinear wave propagation in layered, absorbing fluid media," IEEE Trans. Ultrason. Ferroelect. Freq. Control **67**(1), 81–91 (2020).
[30]Y. Jing, D. Shen, and G. T. Clement, "Verification of the Westervelt equation for focused transducers," IEEE Trans. Ultrason. Ferroelect. Freq. Control **58**(5), 1097–1101 (2011).
[31]B. E. Treeby, J. Jaros, A. P. Rendell, and B. T. Cox, "Modeling nonlinear ultrasound propagation in heterogeneous material using a k-space pseudospectral method," J. Acoust. Soc. Am. **131**(6), 4324–4336 (2012).
[32]J. L. Robertson, B. T. Cox, and B. E. Treeby, "Quantifying numerical errors in the simulation of transcranial ultrasound using pseudospectral methods," in *Proceedings of the 2014 IEEE International Ultrasonics Symposium*, Chicago, IL (September 3–6, 2014).
[33]R. T. Beyer, *Nonlinear Acoustics* (Acoustical Society of America, Woodbury, NY, 1997), pp. 91–164, 165–203, 299–333.
[34]A. B. Vaughn, K. M. Leete, K. L. Gee, B. R. Adams, and J. M. Downing, "Evidence for nonlinear reflections in shock-containing noise near high-performance military aircraft," J. Acoust. Soc. Am. **149**(4), 2403–2414 (2021).
[35]E. A. Zabolotskaya and V. R. Khokhlov, "Quasi-plane waves in the non-linear acoustics of confined beams," Sov. Phys. Acoust. **15**, 35–40 (1969).